Self-consistent rate theory for submonolayer surface growth of multicomponent systems

Mario Einax[*]
School of Chemistry, Tel Aviv University, Tel Aviv 69978, Israel
and Fachbereich Physik, Universität Osnabrück, Barbarastraße 7, 49076 Osnabrück, Germany

Philipp Maass[†]
Fachbereich Physik, Universität Osnabrück, Barbarastraße 7, 49076 Osnabrück, Germany

Wolfgang Dieterich[‡]
Fachbereich Physik, Universität Konstanz, 78457 Konstanz, Germany

(Received 14 March 2014; revised manuscript received 16 June 2014; published 25 July 2014)

The self-consistent rate theory for surface growth in the submonolayer regime is generalized from mono- to multicomponent systems, which are formed by codeposition of different types of atoms or molecules. The theory requires the introduction of pair density distributions to enable a symmetric treatment of reactions among different species. The approach is explicitly developed for binary systems and tested against kinetic Monte Carlo simulations. Using a reduced set of rate equations, only a few differential equations need to be solved to obtain good quantitative predictions for island and adatom densities, as well as densities of unstable clusters.

DOI: 10.1103/PhysRevB.90.035441 PACS number(s): 68.55.A−, 68.43.Jk, 81.15.Aa

I. INTRODUCTION

Growth of solid structures on surfaces, induced by atomic or molecular deposition, has become a widely applied method for generating materials of nanoscale dimensions [1–7]. The resulting clusters or thin films are often metastable, and their structure depends on kinetics rather than thermodynamics. Understanding and controlling such growth processes are prerequisites for designing nanomaterials of practical use. Multicomponent systems are particularly promising in this respect because of their larger structural variability compared to single-component systems [8]. In the submonolayer growth regime, one-monolayer islands can act as seeds for three-dimensional (3D) structures that emerge in later stages of growth [9–12].

Island nucleation and submonolayer growth of binary systems, driven by codeposition of two species A and B, have recently been investigated by using rate equations and kinetic Monte Carlo (KMC) simulations [13]. Generalized relations were established that describe the scaling of stable island densities with the partial fluxes F_α ($\alpha = A$ or B), adatom diffusion coefficients D_α, and mutual binding energies $E_{\alpha\beta}$. Simulations also showed that island density data, when combined for different compositions, enable us to extract microscopic parameters for mixed systems [14]. Of particular value is the possibility to determine the binding energy E_{AB} between unlike atoms in the presence of a surface.

In the rate equations for submonolayer growth [15–17], capture numbers σ_s appear as parameters which determine the attachment rate of diffusing adatoms to islands of size s. Already in the single-component case, it is known that for a quantitative description of island densities as a function of coverage Θ, it is essential to deal with effective capture numbers $\sigma_s(\Theta,\Gamma)$ [18–21]. Their dependence on the coverage Θ and the "D/F ratio," $\Gamma = D/F$, reflects the fact that the efficiency of an island of size s to capture adatoms is affected by the shielding by other islands in its neighborhood. Within a mean-field description of these shielding effects, a central s-sized island is thought to be embedded in an effective medium, characterized by an absorption length ξ for the adatoms. This length describes the capture efficiencies of all islands in an averaged manner. As the rate of capture by the central island is determined by the ξ-dependent adatom density profile in its vicinity, one arrives at a self-consistency condition for σ_s. Originally, this self-consistent theory was formulated for diffusion-limited irreversible growth [22]. Later it was extended to include detachment kinetics [23,24], and to examine capture numbers in the presence of cluster diffusion [25] and adsorbate interactions [26,27].

Our goal here is to generalize the self-consistent theory of diffusion-limited growth to multicomponent systems. To obtain capture numbers that are symmetric under the exchange of species, it is necessary to introduce pair distribution functions. The treatment will be focused on binary systems, where trimers and larger islands are stable irrespective of composition, whereas the stability of dimers AA, AB, and BB is allowed to be composition-dependent. Generalizations are discussed in Sec. VI.

II. RATE EQUATIONS FOR BINARY SYSTEMS

Following earlier work [13,28], we start out from rate equations for island densities in a system of two species, A and B. For simplicity, we will speak about A and B "atoms," but these could also be molecules if their geometrical arrangement with respect to the substrate topology does not play an essential role for the time evolution of island densities. The A and B species are assumed to be deposited as adatoms (no cluster deposition) and to be mobile on the surface. They undergo nucleation and dissociation reactions among themselves, and they attach to and detach from already formed islands of larger

[*]mario.einax@uni-osnabrueck.de
[†]philipp.maass@uni-osnabrueck.de
[‡]wolfgang.dieterich@uni-konstanz.de

size. These larger islands are considered to be immobile. The coverage Θ is supposed to be small enough so that coalescence of islands can be neglected. Direct impingement of arriving atoms onto already existing islands and desorption processes are neglected, or they may be taken into account by introducing properly rescaled fluxes. Furthermore, we limit our discussion to cases in which the largest unstable islands are composed of not more than two atoms. Then the time evolution of adatom densities n_α, $\alpha = A,B$, is given by

$$\frac{dn_\alpha}{dt} = F_\alpha - 2D_\alpha\sigma_1^{\alpha\alpha}n_\alpha^2 - (D_A + D_B)\sigma_1^{AB}n_An_B - D_\alpha n_\alpha\sum_{s\geqslant 2}\sigma_s^\alpha n_s + K_2^{AB}n_{AB} + 2K_2^{\alpha\alpha}n_{\alpha\alpha}. \quad (1)$$

Positive contributions to (1) arise from the partial fluxes $F_\alpha = x_\alpha F$, with x_α the fraction of α atoms and $F = F_A + F_B$ the total flux, and from the decay of the different kinds of dimers with densities $n_{\alpha\beta}$. Negative contributions refer to the formation of dimers and attachment of adatoms to s-sized islands. Note that the diffusion coefficient for the relative motion of A and B is $D_A + D_B$. In the sum over s, the term $s = 2$ involves $n_2 = n_{AA} + n_{AB} + n_{BB}$. The rate equations for dimer densities are

$$\frac{dn_{\alpha\alpha}}{dt} = D_\alpha\sigma_1^{\alpha\alpha}n_\alpha^2 - \left(\sum_\beta D_\beta\sigma_2^\beta n_\beta\right)n_{\alpha\alpha} - K_2^{\alpha\alpha}n_{\alpha\alpha}, \quad (2)$$

$$\frac{dn_{AB}}{dt} = (D_A + D_B)\sigma_1^{AB}n_An_B - \left(\sum_\beta D_\beta\sigma_2^\beta n_\beta\right)n_{AB} - K_2^{AB}n_{AB}. \quad (3)$$

The upper indices in the capture numbers $\sigma_1^{\alpha\beta}$,σ_s^α and decay rates $K_2^{\alpha\beta}$ serve to distinguish the types of adatoms that are involved in a reaction. The $\sigma_1^{\alpha\beta}$ and $K_2^{\alpha\beta}$, respectively, refer to formation and dissociation of an $\alpha\beta$ dimer. The σ_s^α, $s \geqslant 2$, refers to the capture of an α adatom by an island composed of s atoms. The geometry of such an island is represented by a circular shape (formation of compact islands) with radius $\mathcal{R}_s = s^{1/2}\mathcal{R}_1$, where $\mathcal{R}_1$ is the adatom radius. Since we allow composition-dependent ("mixed") dimer stabilities, some of the decay rates can be zero. For the purpose of calculating n_α, $n_{\alpha\beta}$, and the total density of stable islands, N, it appears sufficient to ignore any further composition dependencies of parameters beyond those given in Eqs. (2) and (3).

The densities of islands with $s > 2$ evolve according to

$$\frac{dn_s}{dt} = \sum_\alpha D_\alpha n_\alpha\left(\sigma_{s-1}^\alpha n_{s-1} - \sigma_s^\alpha n_s\right). \quad (4)$$

III. IRREVERSIBLE GROWTH

In the self-consistent rate theory, analytical expressions for the capture numbers and decay rates are derived by introducing an effective medium that describes adatom capture in an averaged manner by an absorption length ξ. For binary systems, the effective medium is characterized by two different absorption lengths ξ_α for the two species of adatoms. To define ξ_α, the evolution equations (1) for monomer densities with zero decay terms ($i = 1$) are rewritten as

$$\frac{dn_\alpha}{dt} = F_\alpha - \frac{1}{\tau_\alpha}n_\alpha, \quad (5)$$

where $\tau_\alpha^{-1} = D_\alpha/\xi_\alpha^2$ is the reaction rate of α adatoms in the effective medium, and

$$\xi_\alpha^{-2} = \sum_\beta(1-\delta_{\alpha\beta})\sigma_1^{\alpha\beta}\left(1 + \frac{D_\beta}{D_\alpha}\right)n_\beta + 2\sigma_1^{\alpha\alpha}n_\alpha + \sum_{s\geqslant 2}\sigma_s^\alpha n_s. \quad (6)$$

Deposition, diffusion, and absorption of adatoms within the effective medium are described by local densities $\tilde{n}_\alpha(\mathbf{r})$ with $n_\alpha = \int_V d^2r\,\tilde{n}_\alpha(\mathbf{r})/V$, where V is the two-dimensional volume (surface area). These satisfy

$$\frac{\partial\tilde{n}_\alpha}{\partial t} = F_\alpha + D_\alpha\Delta\tilde{n}_\alpha - \frac{1}{\tau_\alpha}\tilde{n}_\alpha. \quad (7)$$

In the monocomponent case, one would have just one equation of this type, and by supplementing this with appropriate boundary conditions, the stationary density profiles of adatoms around islands with radius R_s can be calculated and the total adatom flux to the islands identified with the corresponding capture terms in Eqs. (1). This procedure yields self-consistent analytical expressions for the capture numbers and decay rates in the monocomponent case.

For binary (multicomponent) systems, the reaction between unlike adatoms needs a refined treatment. This is due to the following reason: In a naive extension of the monocomponent case, the B adatom density around an A adatom would by characterized by an absorption length ξ_B, and the A adatom density around a B adatom by an absorption length ξ_A. However, the shape of both profiles is given by the pair density $n_{AB}(\mathbf{r},\mathbf{r}')$ of A and B adatoms, and hence the profiles must be characterized by the same capture length (if inversion symmetry holds). In fact, introducing the pair distribution function [29,30]

$$G_{AB}(\mathbf{r}) = \frac{1}{V}\int_V d^2r'\int_V d^2r''\,n_{AB}(\mathbf{r}',\mathbf{r}'')\delta(\mathbf{r} - (\mathbf{r}' - \mathbf{r}'')) \quad (8)$$

allows one to treat unlike adatoms in a symmetric way, resulting in a symmetric expression for σ_1^{AB}. $G_{AB}(\mathbf{r})$ is the number of pairs of A and B adatoms at distance $\mathbf{r}$ per area. Let us note that the approach based on pair distribution functions is well known in the kinetic theory of bimolecular chemical reactions [30,31]. In our context, spatial correlations between adatoms for relative distances larger than the contact distance $R_1 = 2\mathcal{R}_1$ play no role so that

$$n_{AB}(\mathbf{r},\mathbf{r}') = \tilde{n}_A(\mathbf{r})\tilde{n}_B(\mathbf{r}'), \quad |\mathbf{r} - \mathbf{r}'| > R_1. \quad (9)$$

Combination with (7) yields an expression for the time derivative of $n_{AB}(\mathbf{r},\mathbf{r}')$. Subsequent multiplication by

$\delta(\mathbf{r}-(\mathbf{r}'-\mathbf{r}''))$ and integration over all $\mathbf{r}'$ and $\mathbf{r}''$ gives

$$\frac{\partial G_{AB}(\mathbf{r})}{\partial t} = F_A n_A + F_B n_B + (D_A + D_B)\Delta G_{AB}(\mathbf{r}) - \left(\frac{1}{\tau_A}+\frac{1}{\tau_B}\right) G_{AB}(\mathbf{r}). \quad (10)$$

Subtracting $d(n_A n_B)/dt$ with the help of Eqs. (5) and going over to the quasistationary limit, we obtain

$$(D_A + D_B)\Delta G_{AB}(\mathbf{r}) = \left(\frac{1}{\tau_A}+\frac{1}{\tau_B}\right)[G_{AB}(\mathbf{r}) - n_A n_B]. \quad (11)$$

Alternatively,

$$\Delta G_{AB}(\mathbf{r}) - \frac{1}{\xi_{\rm eff}^2}[G_{AB}(\mathbf{r}) - n_A n_B] = 0, \quad (12)$$

where we introduced the effective absorption length

$$\xi_{\rm eff}^{-2} = \frac{1}{D_A + D_B}\left(\frac{D_A}{\xi_A^2}+\frac{D_B}{\xi_B^2}\right), \quad (13)$$

which is a weighted average of ξ_α^{-2}, with weighting factors $D_\alpha/(D_A + D_B)$.

For $i = 1$, implying complete absorption at contact, and assuming isotropy, the boundary conditions to Eq. (12) are

$$G_{AB}(r) \to \begin{cases} n_A n_B, & r \to \infty, \\ 0, & r \to R_1, \end{cases} \quad (14)$$

where $r = |\mathbf{r}|$, and we have replaced $G_{AB}(\mathbf{r})$ by $G_{AB}(r)$. The solution of Eq. (12) with the boundary conditions in Eq. (14) is $G_{AB}(r) = n_A n_B[1 - \mathcal{K}_0(r/\xi_{\rm eff})/\mathcal{K}_0(R_1/\xi_{\rm eff})]$, where $\mathcal{K}_\nu$ is the modified Bessel function of order ν.

To obtain the reaction rate, we first select reactions along a particular direction $\hat{\mathbf{r}} = \mathbf{r}/|\mathbf{r}|$, $\mathbf{r}$ being the relative coordinate between an A and B atom right before contact. The corresponding rate is given by

$$I(\hat{\mathbf{r}}) = \lim_{|\mathbf{r}|\to R_1} \frac{1}{V}\int d^2r' \int d^2r''\, \hat{\mathbf{r}}\cdot[\mathbf{j}_B(\mathbf{r}'')\tilde{n}_A(\mathbf{r}') - \mathbf{j}_A(\mathbf{r}')\tilde{n}_B(\mathbf{r}'')]\,\delta(\mathbf{r}-(\mathbf{r}'-\mathbf{r}'')), \quad (15)$$

where $\mathbf{j}_\alpha(\mathbf{r}) = -D_\alpha \nabla \tilde{n}_\alpha(\mathbf{r})$. Substituting this expression into (15) and using (8), we can reexpress (15) as $I(\hat{\mathbf{r}}) = (D_A + D_B)(\partial G_{AB}/\partial r)|_{R_1}$. After integration along the boundary at $r = R_1$, we obtain the total number of reactions per second and per unit area, which is identified with the corresponding term in the original rate equations, $(D_A + D_B)\sigma_1^{AB} n_A n_B$. Thus, we obtain

$$\sigma_1^{AB} = 2\pi R_1 \frac{1}{n_A n_B}\left(\frac{\partial G_{AB}}{\partial r}\right)_{R_1}. \quad (16)$$

Evidently, this result for AB capture in a binary system has a structure analogous to the self-consistent capture number σ_1 for a one-component system of overall adatom density n and diffusion coefficient D. That situation and the present one can be mapped onto each other by $n \leftrightarrow n_A n_B$; $2D \leftrightarrow D_A + D_B$; $\tilde{n}(\mathbf{r}) \leftrightarrow G_{AB}(\mathbf{r})$ for the local densities in the SCF treatment, and $\xi \leftrightarrow \xi_{\rm eff}$, where $\xi_{\rm eff}$ was defined by (13). Hence we can immediately translate known results for one-component systems to the present case, to obtain

$$\sigma_1^{AB} = 2\pi \frac{R_1}{\xi_{\rm eff}} \frac{\mathcal{K}_1(R_1/\xi_{\rm eff})}{\mathcal{K}_0(R_1/\xi_{\rm eff})}. \quad (17)$$

The $\sigma_1^{\alpha\alpha}$ are obtained by introducing the pair correlation function $G_{\alpha\alpha}(r)$ for like particles and repeating the above steps. For $\sigma_1^{\alpha\alpha}$, we recover the form (17) with $\xi_{\rm eff}$ replaced by ξ_α. Moreover, we need σ_s^α for $s \geqslant 2$. Since islands with $s \geqslant 2$ do not move, the result is again equivalent to (17), where one type of adatom has a zero diffusion coefficient. For example, σ_s^A is given by (17) with $D_B = 0$, hence $\xi_{\rm eff} = \xi_A$, and R_1 is replaced by $R_s = \mathcal{R}_s + \mathcal{R}_1$. Clearly, our treatment also covers one-component systems through the limit where A and B atoms become indistinguishable.

IV. DECAY PROCESSES

In this section, we extend the above scheme to include detachment processes. First, we focus on unstable AB dimers, characterized by some finite binding energy E_{AB} [14]. This situation can be incorporated into the treatment of Sec. III by a modification of the boundary condition (14). Consider detachment and reattachment reactions between an A and B adatom. Within a lattice model and E_{AB} a nearest-neighbor binding energy, the bound state corresponds to an AB pair located on nearest-neighbor sites, whereas in the detached state the A and B adatoms are separated by one vacant site. We denote by n_{AB} and n_{AB}^* the densities of bound and detached states of this type. Assuming local equilibrium, both densities are related by

$$n_{AB}^* = n_{AB}\,\mu_{AB}\,\exp(-E_{AB}/k_{\rm B}T). \quad (18)$$

The factor μ_{AB} is determined by the degeneracies of the bound and dissociated states in a circularly averaged description, and it depends on the geometry of A and B adsorption sites on the surface. We do not go into the underlying counting problem for specific lattice geometries [24], but merely treat μ_{AB} as a parameter [13]. Writing $\mu_{AB}\exp(-E_{AB}/k_{\rm B}T) = \kappa_{AB}$, we arrive at the local equilibrium boundary condition,

$$G_{AB}(r) \to \kappa_{AB}\, n_{AB}, \quad r \to R_2. \quad (19)$$

As before, see Eq. (14), $G_{AB}(r) \to n_A n_B$ as $r \to \infty$. Solving Eq. (12) for these boundary conditions yields $G_{AB}(r) = n_A n_B[1 - \zeta\mathcal{K}_0(r/\xi_{\rm eff})/\mathcal{K}_0(R_1/\xi_{\rm eff})]$ with $\zeta = (1 - \kappa_{AB} n_{AB}/n_A n_B)$.

The total reaction rate can be then written as [23]

$$I_{\rm tot} = I_{\rm capture} - I_{\rm decay}, \quad (20)$$

where $I_{\rm capture} = (D_A + D_B)\sigma_1^{AB} n_A n_B$ is defined with σ_1^{AB} from Eq. (16), and

$$I_{\rm decay} = \frac{n_{AB}}{n_A n_B}\kappa_{AB} I_{\rm capture}. \quad (21)$$

Identifying with the corresponding decay term $K_2^{AB} n_{AB}$ in Eq. (3), we find

$$K_2^{AB} = (D_A + D_B)\kappa_{AB}\sigma_1^{AB}. \quad (22)$$

In the same way, we obtain

$$K_2^{\alpha\alpha} = 2D_\alpha \kappa_{\alpha\alpha}\sigma_1^{\alpha\alpha} \quad (23)$$

with $\kappa_{\alpha\alpha} = \mu_{\alpha\alpha} \exp(-E_{\alpha\alpha}/k_B T)$. Again, the degeneracy factors $\mu_{\alpha\alpha}$ are treated as parameters.

Note that when we use these results for the self-consistent capture and decay numbers in the two-component Walton relations [13], $(D_A + D_B)\sigma_1^{AB} n_A n_B \simeq K_2^{AB} n_{AB}$, it follows that $I_{\text{capture}} \simeq I_{\text{decay}}$. This is consistent with the quasistationarity assumption underlying the Walton relations [32], which implies that the capture and decay rates nearly balance. Let us further note that reaction barriers for formation and dissociation of dimers can also be incorporated in the treatment. They lead to a modification of the boundary condition (19), corresponding to a partially reflecting boundary, sometimes called the "radiative boundary condition" [23,31,33].

V. NUMERICAL RESULTS AND DISCUSSION

The coupled set of rate equations (1)–(4) along with the self-consistent expressions for the capture numbers must be solved numerically by using an iterative integration scheme. An adequate but time-consuming numerical integration requires solving a large number of equations for an s-range in Eqs. (4) significantly exceeding the mean island size $\bar{s} = \Theta/N$. A much simpler approach of almost the same quality has been proposed for one-component systems by Venables [15], and it can be applied to the binary mixtures considered here. In the case $i = 1$, where $K_2^{\alpha\beta} = 0$, this approach amounts to setting

$$\sum_{s \geqslant 2} \sigma_s^\alpha n_s = \bar{\sigma}^\alpha N \tag{24}$$

in Eq. (6), to be combined with Eq. (5). Here, $\bar{\sigma}^\alpha$ is the average capture number of stable clusters. Inserting the results from Sec. III for σ_s^α [see the discussion following Eq. (17)] and assuming that n_s is sufficiently peaked around the mean island size $\bar{s}$, one obtains

$$\bar{\sigma}^\alpha = 2\pi \frac{\bar{R}}{\xi_\alpha} \frac{\mathcal{K}_1(\bar{R}/\xi_\alpha)}{\mathcal{K}_0(\bar{R}/\xi_\alpha)}, \tag{25}$$

where $\bar{R} = R_{\bar{s}} = (\bar{s}^{1/2} + 1)\mathcal{R}_1$. The self-consistency problem then reduces to solving three coupled equations, Eq. (5) for $\alpha = A$ and B, and the equation for nucleation of stable clusters,

$$\frac{dN}{dt} = \sum_\alpha D_\alpha \sigma_1^{\alpha\alpha} n_\alpha^2 + (D_A + D_B)\sigma_1^{AB} n_A n_B. \tag{26}$$

Capture numbers $\sigma_1^{\alpha\beta}$ and $\bar{\sigma}^\alpha$ entering these equations become functions of n_α and N.

In the more general case of Sec. IV, allowing dimer decay processes, we must distinguish between stable and unstable dimers. The example considered below refers to unstable BB dimers but stable AA and AB dimers, which entails the decomposition

$$\sum_{s \geqslant 2} \sigma_s^\alpha n_s = \sigma_2^\alpha n_{BB} + \overline{\sigma}^\alpha N. \tag{27}$$

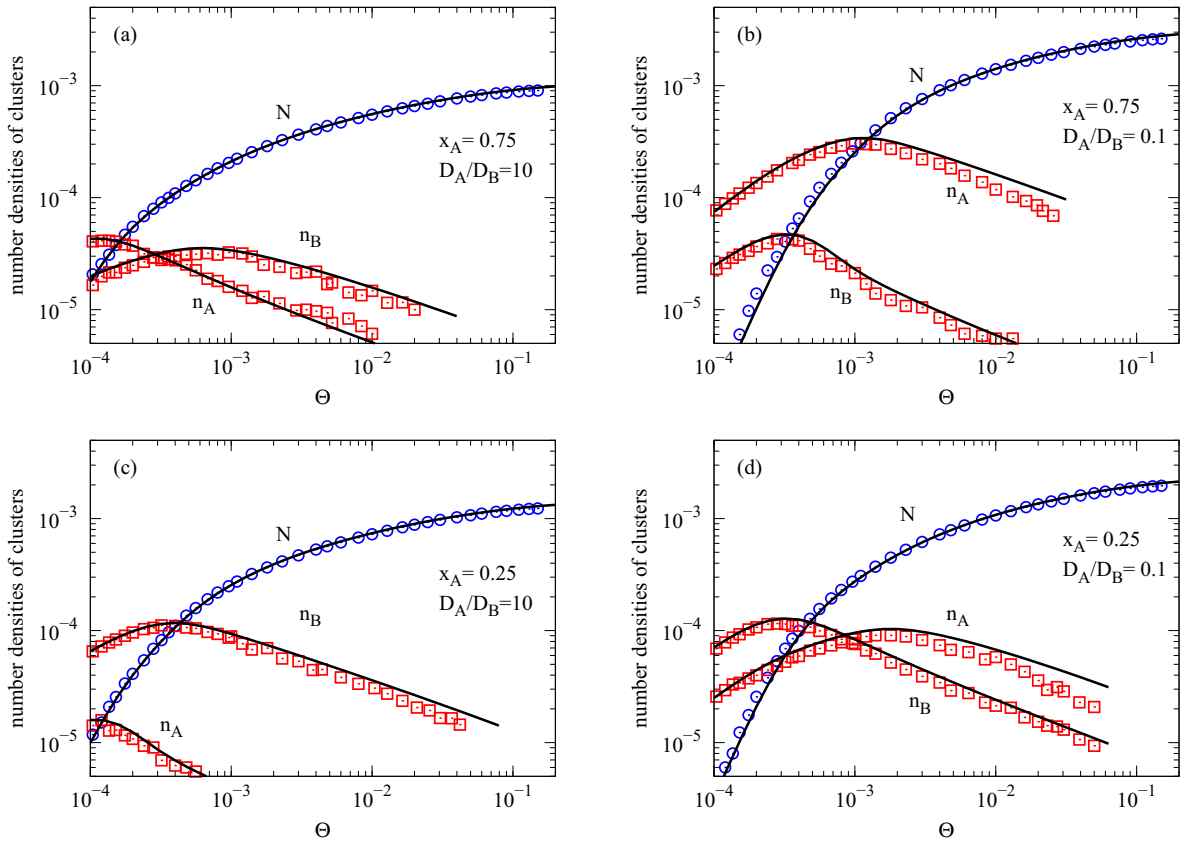

FIG. 1. (Color online) Number densities of A and B adatoms, and stable islands as a function of the coverage $\Theta = Ft$ for $i = 1$ and various combinations of x_A and D_A/D_B. Results from the self-consistent rate theory are given by solid lines.

The relevant rate equations now include Eq. (2) for $\alpha = B$ and

$$\frac{dN}{dt} = D_A \sigma_1^{AA} n_A^2 + (D_A + D_B)\sigma_1^{AB} n_A n_B + \left(D_A \sigma_2^A n_A + D_B \sigma_2^B n_B\right) n_{BB} \quad (28)$$

instead of (26).

To test the self-consistent theory based on that reduced set of coupled rate equations, we have performed KMC simulations for codeposition of A and B atoms onto a triangular lattice with 500×500 sites at various compositions and D_A/D_B ratios, and for different situations of cluster stabilities with respect to their size and composition. Monomers of size $\mathcal{R}_1 = a$ ($R_1 = 2\mathcal{R}_1 = 2a$) are deposited at random to vacant substrate sites, where $a = 1$ is the lattice constant, and they diffuse via nearest-neighbor hops, excluding multiple site occupation. Attachment of monomers to islands is accompanied by instantaneous relaxation to highly coordinated edge sites, yielding compact cluster structures. For each parameter set, the number densities were averaged over 50 realizations. Compact cluster morphologies have the advantage over fractal ones that the self-consistent theory can be tested over a wider range of coverages, because the coalescence regime starts later.

First, we study the situation of irreversible growth, $i = 1$. Results for N and n_α are plotted in Fig. 1 as a function of the coverage $\Theta = Ft$ for two concentrations $x_A = 0.75$ and 0.25. In the simulations for both concentrations, $D_B/F = 10^7$ was fixed, and two values $D_A = 10D_B$ and $0.1D_B$ were considered. The reduced self-consistent theory without fitting parameters (solid lines) evidently is in good quantitative agreement with the KMC simulations (open symbols). At low coverages (short times), $n_\alpha = x_\alpha \Theta$, whereas in the scaling regime (see the discussion in Refs. [4,8]), $n_\alpha \simeq x_\alpha F/D_\alpha N$ [13,28]. By going from Figs. 1(a) to 1(b), the diffusion coefficient of the majority component A is lowered by a factor 10^2, which explains the fact that n_A gets much larger than n_B and the corresponding curves do not intersect anymore. Inspection of Eq. (26) in turn shows that nucleation of stable islands in Fig. 1(a) is mostly due to the second term, i.e., nucleation of AB dimers prevails, whereas in Fig. 1(b) both AA and AB dimers will appear with similar densities. In Fig. 1(b), N close to saturation becomes significantly larger than in Fig. 1(a), which is consistent with the scaling form $N \propto (\Gamma_{\rm eff})^{-1/3}$ with $\Gamma_{\rm eff} = (\sum_\alpha x_\alpha F/D_\alpha)^{-1}$ [13,28]. For $x_A = 0.25$ [Figs. 1(c) and 1(d)], the influence of the mobility ratio D_A/D_B on N is less pronounced. Nucleation in Fig. 1(c) proceeds mainly by the formation of BB dimers.

Next we include detachment kinetics. Specifically, we assume that the stability of dimers depends on their composition: AA and AB dimers are stable ($K_2^{AA} = K_2^{AB} = 0$), while BB dimers are unstable with zero binding energy. The parameter μ_{BB} was set to $\mu_{BB} = 0.1$ [34]. The number density of stable islands is given by $N = n_{AA} + n_{AB} + \sum_{s>2} n_s$ and its time evolution obeys Eq. (28). Again, numerical results based on

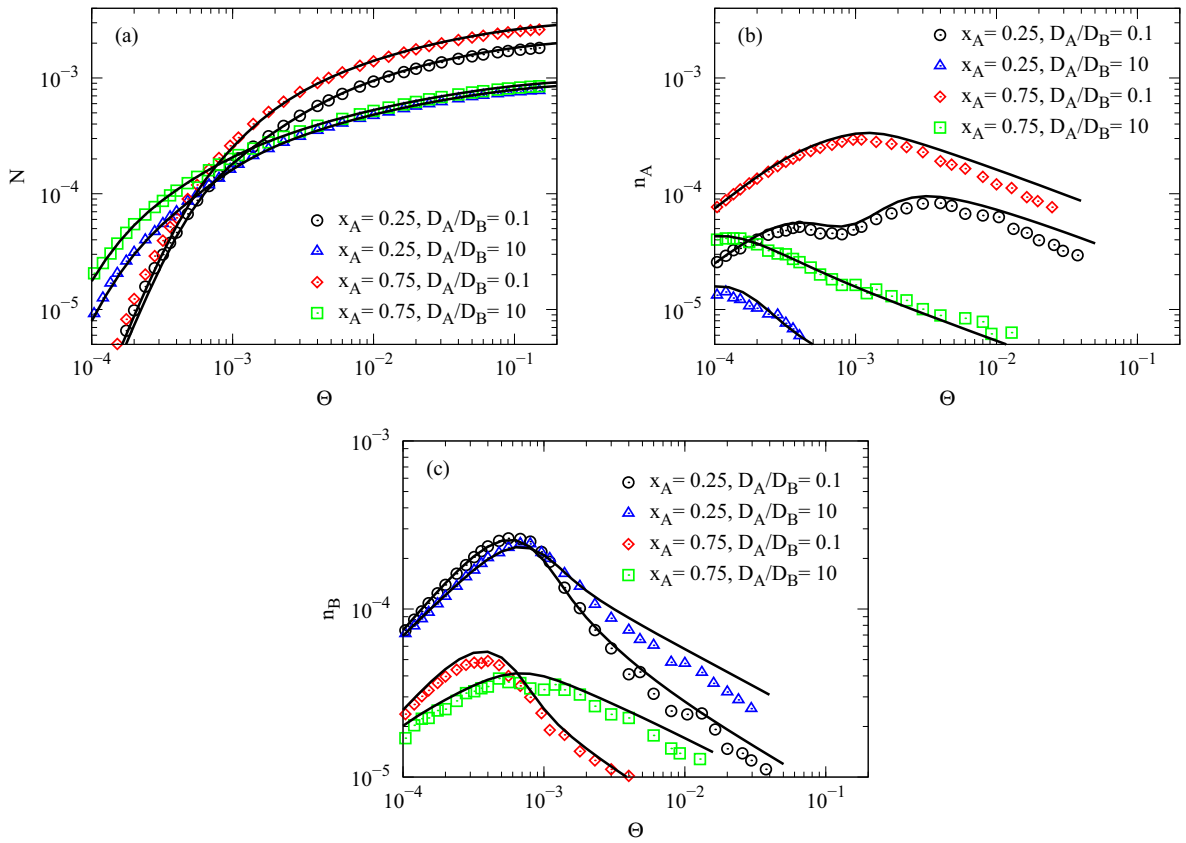

FIG. 2. (Color online) Number densities of (a) stable islands N, (b) A adatoms, and (c) B adatoms as a function of the coverage Θ for a case of mixed dimer stabilities, where AA and AB dimers are stable while BB dimers are unstable with zero binding energies. Results from the self-consistent approach (solid lines) with $\mu_{BB} = 0.1$ are compared with KMC simulations (symbols).

our self-consistent rate equations for mixtures are in good quantitative agreement with the KMC simulations. This is shown in Figs. 2(a)–2(c) and Figs. 3(a) and 3(b) for the same values of x_A and D_α as considered in Fig. 1.

A feature worth noting in Fig. 2(b) is the occurrence of a local minimum of n_A as a function of Θ for $x_A = 0.25$ and $D_A/D_B = 0.1$. It can be understood as follows. For these parameters and throughout the nucleation regime, AB nucleation is the dominating process for capture of A atoms; see Figs. 3(a) and 3(c). The reason is that BB dissociation entails a large number of B adatoms, as can be seen in Fig. 2(c): The peak in n_B near $\Theta \simeq 10^{-3}$ is about 2.5 times higher than the corresponding peak in Fig. 1(d) in the absence of dissociation. When, with increasing Θ, the B adatom density n_B approaches its maximum, AB nucleation becomes strong enough to overcome the gain of n_A by the external flux F_A, hence n_A gets depleted. Beyond $\Theta \simeq 10^{-3}$, on the other hand, n_B quickly decreases due to reactions with stable islands so that n_A, after going through a minimum, can increase again through deposition with F_A. Upon further increasing Θ, it passes a second maximum and finally drops through absorption by stable islands.

Shortly speaking, the consumption of n_A after its first maximum in Fig. 2(b) is governed by AB nucleation, and after its second maximum by attachments to stable islands. The rise of the A adatom density after the minimum is due to missing B adatoms for AB nucleation and the small D_A value. From this discussion it should become clear why the minimum is not seen for the curves with the larger value $D_A/D_B = 10$ (shorter mean time to traverse the mean free path) or the larger $x_A = 0.75$ (smaller mean free path for AA nucleation).

To discuss nucleation rates based on Eq. (28) and the self-consistent theory, note first that in all our examples nucleation of trimers via BB dimers is rare, because n_{BB} is small due to decay processes. Therefore, the last term in Eq. (28) is negligible. The remaining two terms, giving the partial rates for nucleation via AA and AB dimers, are represented in Fig. 3(c) by open and filled symbols, respectively. For example, for $x_A = 0.75$ and $D_A/D_B = 0.1$, the term $2D_A\sigma_1^{AA}(n_A)^2$ (open diamonds) becomes larger than the term $(D_A + D_B)\sigma_1^{AB}n_An_B$ (filled diamonds). The formation of stable islands [open diamonds in Fig. 2(a)] is therefore caused mostly by the nucleation path via AA dimers. By contrast, for $x_A = 0.25$ and $D_A/D_B = 10$ we observe the opposite scenario [see the open and filled triangles in Fig. 3(c)], which means that AB nucleation prevails. In the remaining two cases in Figs. 2 and 3, both the AA and the AB dimer route contribute with similar strength to the formation of stable islands.

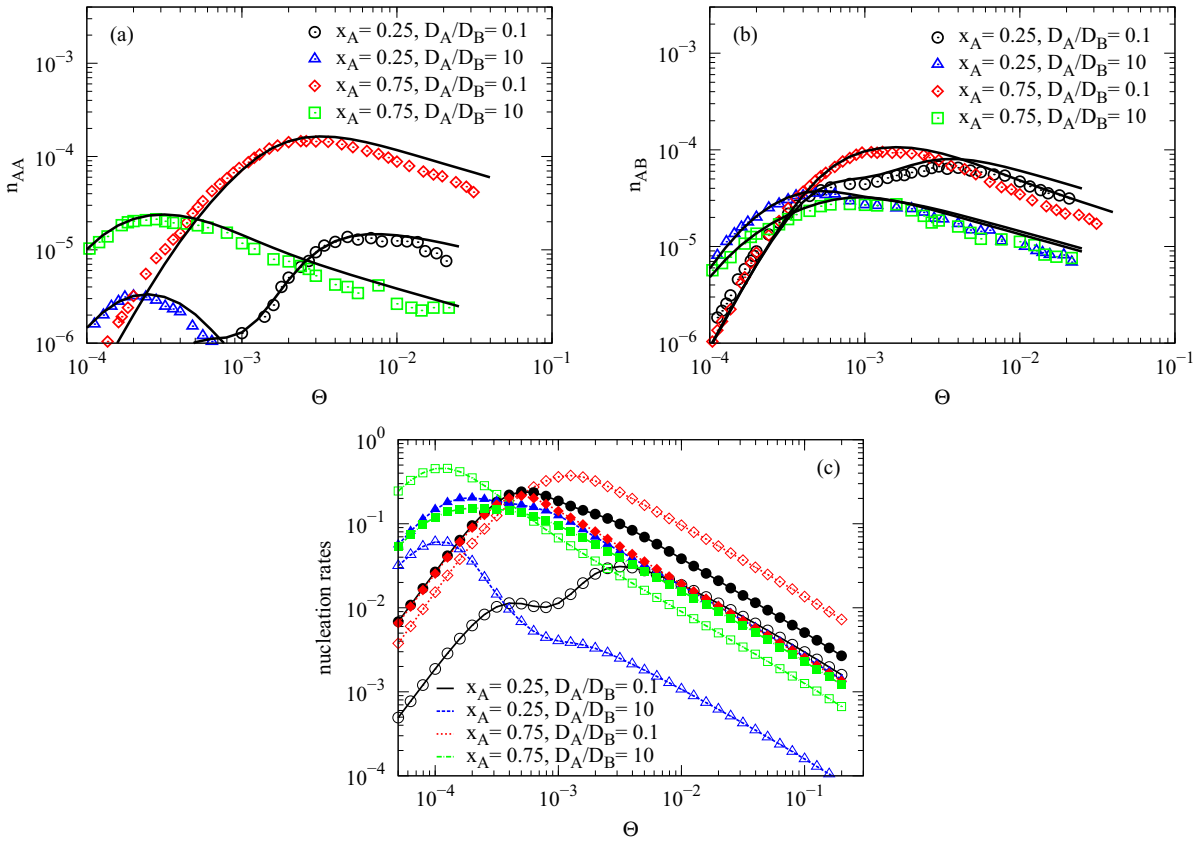

FIG. 3. (Color online) Densities of (a) stable AA dimers, (b) stable AB dimers, and (c) partial nucleation rates $2D_A\sigma_1^{AA}(n_A)^2$ (open symbols) and $(D_A + D_B)\sigma_1^{AB}n_An_B$ (filled symbols) as a function of the coverage Θ for mixed dimer stabilities as in Fig. 2. In (a) and (b) the symbols refer to KMC results, and in (c) they are used for the assignment of the lines to the parameters. In all figure parts, the lines represent results of the self-consistent rate theory.

VI. CONCLUSIONS

We have shown that a self-consistent treatment of capture numbers in the rate equations for surface growth of binary systems yields a very good quantitative description of island and adatom densities. Essential for this theory is the effective absorption length ξ_{eff} in Eq. (13), which is symmetric in the two components A and B. Its derivation requires the introduction of pair densities. Note that the weighting factors $D_\alpha/(D_A + D_B)$ appearing in that equation can strongly vary with temperature as the underlying activation energies for the two species generally differ. In this way, ξ_{eff} acquires an additional temperature dependence that we expect to become important in measurements of island and adatom densities.

Different scenarios for dimer stabilities and prevailing nucleation routes were studied. In all cases, only a reduced set of few coupled rate equations needs to be solved, which can easily be done on a PC.

Extensions of our theoretical treatment to larger unstable clusters is straightforward by first generalizing the rate equations as described in Ref. [13]. Reduced sets of coupled rate equations comprise the densities of stable islands, monomers, and all unstable clusters. Extensions to systems with more than two components and (as before) pairwise reactions follow directly from the above scheme by introducing pair densities $G_{\alpha\beta}(\mathbf{r})$ among all mobile adatom species α and associated effective absorption lengths $\xi_{\alpha\beta}$. More generally, in the case of nonvanishing cluster mobilities [35], pair densities need to be introduced for all pairs of mobile species.

In our treatment, we have neglected strain effects so far, which, however, can have a significant influence on the kinetic growth behavior. It would be interesting, therefore, to further extend the present pair density formulation, for example by taking into account a strain-induced shift in the barrier [36,37] for monomer migration.

[1] H. Brune, Surf. Sci. Rep. **31**, 125 (1998).
[2] C. Ratsch and J. A. Venables, J. Vac. Sci. Technol. A **21**, S96 (2003).
[3] T. Michely and J. Krug, *Islands, Mounds and Atoms: Patterns and Processes in Crystal Growth Far from Equilibrium* (Springer, Berlin, 2004).
[4] J. W. Evans, P. A. Thiel, and M. C. Bartelt, Surf. Sci. Rep. **61**, 1 (2006).
[5] A. Kühnle, Curr. Opin. Colloid Interface Sci. **14**, 157 (2009).
[6] G. Hlawacek and C. Teichert, J. Phys.: Condens. Matter **25**, 143202 (2013).
[7] P. Rahe, M. Kittelmann, J. L. Neff, M. Nimmerich, M. Reichling, P. Maass, and A. Kühnle, Adv. Mater. **25**, 3948 (2013).
[8] M. Einax, W. Dieterich, and P. Maass, Rev. Mod. Phys. **85**, 921 (2013).
[9] M. Körner, F. Loske, M. Einax, A. Kühnle, M. Reichling, and P. Maass, Phys. Rev. Lett. **107**, 016101 (2011).
[10] M. Albrecht, M. Maret, A. Maier, F. Treubel, B. Riedlinger, U. Mazur, G. Schatz, and S. Anders, J. Appl. Phys. **91**, 8153 (2002).
[11] F. Liscio, M. Maret, C. Meneghini, S. Mobilio, O. Proux, D. Makarov, and M. Albrecht, Phys. Rev. B **81**, 125417 (2010).
[12] M. Einax, S. Heinrichs, P. Maass, A. Majhofer, and W. Dieterich, J. Phys.: Condens. Matter **19**, 086227 (2007).
[13] M. Einax, S. Ziehm, W. Dieterich, and P. Maass, Phys. Rev. Lett. **99**, 016106 (2007).
[14] M. Einax, W. Dieterich, and P. Maass, J. Appl. Phys. **105**, 054312 (2009).
[15] J. A. Venables, Philos. Mag. **27**, 697 (1973).
[16] J. A. Venables, G. D. T. Spiller, and M. Hanbücken, Rep. Prog. Phys. **47**, 399 (1984).
[17] J. A. Venables, *Introduction to Surface and Thin Film Processes* (Cambridge University Press, Cambridge, 2000).
[18] F. Gibou, C. Ratsch, and R. Caflisch, Phys. Rev. B **67**, 155403 (2003).
[19] M. N. Popescu, J. G. Amar, and F. Family, Phys. Rev. B **64**, 205404 (2001).
[20] M. Körner, M. Einax, and P. Maass, Phys. Rev. B **82**, 201401(R) (2010).
[21] M. Körner, M. Einax, and P. Maass, Phys. Rev. B **86**, 085403 (2012).
[22] G. S. Bales and D. C. Chrzan, Phys. Rev. B **50**, 6057 (1994).
[23] G. S. Bales and A. Zangwill, Phys. Rev. B **55**, R1973 (1997).
[24] M. N. Popescu, J. G. Amar, and F. Family, Phys. Rev. B **58**, 1613 (1998).
[25] B. C. Hubartt, Y. A. Kryukov, and J. G. Amar, Phys. Rev. E **84**, 021604 (2011).
[26] J. A. Venables and H. Brune, Phys. Rev. B **66**, 195404 (2002).
[27] S. Ovesson, Phys. Rev. Lett. **88**, 116102 (2002).
[28] W. Dieterich, M. Einax, and P. Maass, Eur. Phys. J. Spec. Top. **161**, 151 (2008).
[29] J. P. Hansen and I. R. McDonald, *Theory of Simple Liquids* (Academic Press, London, 1986).
[30] E. A. Kotomin and V. N. Kuzovkov, *Modern Aspects of Diffusion-Controlled Processes: Cooperative Phenomena in Bimolecular Reactions*, edited by R. G. Compton and G. Hancock, Chemical Kinetics Vol. 34 (North Holland, Amsterdam, 1996).
[31] T. R. Waite, Phys. Rev. **107**, 463 (1957).
[32] D. Walton, J. Chem. Phys. **37**, 2182 (1962).
[33] D. Kandel, Phys. Rev. Lett. **78**, 499 (1997).
[34] From the corresponding counting problem for specific lattice geometries [24], the estimate $\mu_{BB} \simeq 0.067$ is obtained, and from fits of the standard rate equations to KMC simulations [13,38], $\mu_{BB} \simeq 0.08$ can be estimated.
[35] P. Jensen, L. Bardotti, V. D. N. Combe, P. Mélinon, B. Pével, J. Tuaillon-Combes, and A. Perez, in *Nanoclusters and Nanocrystals*, edited by H. S. Nalwa, Advances in Nanophase Materials and Nanotechnology (American Scientific Publishers, Los Angeles, 2003), Chap. 4.
[36] G. Nandipati and J. G. Amar, Phys. Rev. B **73**, 045409 (2006).
[37] C. Ratsch, J. DeVita, and P. Smereka, Phys. Rev. B **80**, 155309 (2009).
[38] J. G. Amar and F. Family, Surf. Sci. **382**, 170 (1997).